

Supporting Information

Mapping multiple plexcitons in disk supershape hybrid nanoparticles

Emadoddin Yaghooti ^a, Ferydon Babaei ^{a,*}, Renming Liu ^{b,c}

^a) Department of Physics, University of Qom, Qom, Iran

^b) Key Laboratory for High Efficiency Energy Conversion and Technology of Henan Province, International Joint Research Laboratory of New Energy Materials and Devices of Henan Province, School of Physics and Electronics, Henan University, Kaifeng 475004, China

^c) Institute of Quantum Materials and Physics, Henan Academy of Sciences, Zhengzhou 450046, China

*) Email: fbabaei@qom.ac.ir

Abstract

In this Supporting Information we enclose a full discussion for core-shell (CS) and bilayer (BL) nanoparticles with geometries as elliptical (a_2), triangular (a_3), cuboidal (a_4), hexapod, (b_2), heptapod (b_3), and octapod (b_4), 4-arms (c_2), 6-arms (c_3), and 7-arms (c_4).

Discussion

Extinction spectra of elliptical metal core, elliptical j-aggregate shell, elliptical CS and BL nanoparticles (circular sublayer/elliptical shell superlayer) are shown in Fig.S1. In Fig.S1a, it is clear that as the size of the metal core increases, the plasmon peaks shift to lower energies and also the width of peaks decreases and their localization increase. Accumulation of electric surface charge density at the vertices is high due to being aligned with the incident electric field. For the size of 30 nm, the electric field at the energy of 2.109 eV is shown as an inset plot, which indicates the formation of hot spots at the vertices. Here, similar to Fig.3, there is a clear plasmonic mode. In Fig.S1b, for an elliptical j-aggregate shell, there are two excitonic peaks, bonding and antibonding, both of which shift to lower energies with the increase of the hole size of the shell. Specifically, for the hole size of 30 nm, the pattern of the electric field at 2.116 and 2.160 eV has been shown, which is clear that they are enhanced at the edges of the shell

and some points inside the shell, respectively. There are three plexitonic modes in Fig.S1c, which are formed by the hybridization of one plasmonic mode from the core and two excitonic modes from the j-aggregate shell. By increasing the size of the core, the intensity of the hybrid modes increases and shifts to lower energies. The electric fields for a sample are shown in two specific energies, whose pattern is different from the electric fields of a bare core and a bare j-aggregate shell. We observed the same behavior for a BL nanoparticle in Fig.S1d.

In Fig.S2, the extinction spectra of a triangular bare metal core, a triangular j-aggregate shell, a triangular CS and a BL nanoparticle (circular sublayer /triangular shell superlayer) are depicted. By increasing the size of the core from 10 to 40 nm in Fig.S2a, the plasmon peaks change to lower energies in the range of 1.987 to 1.616 eV. Meanwhile, the plasmonic peaks become narrower and their intensity increases. In this structure, there is almost a clear plasmonic peak, which its electric field is shown for the core size of 30 nm at the energy of 1.722 eV. As it is known, the hottest spot is formed in the left arc because a longer length of this arc is exposed to the incident electric field, although there are also the hot spots in the two right arcs with less surface charge density. From Fig.S2b, it is clear that there are two excitonic peaks for a triangular j-aggregate shell, both of which move to lower energies as the hole size increases. The electric fields of them are drawn for a shell with 30 nm air hole. It can be seen from the pattern of electric fields for the mentioned sample that at the energy of 2.109 eV electron volts (dimeric band), hot spots are formed on the arcs, while at the energy of 2.153 eV (monomeric band), hot spots are formed between the arcs. From the entanglement of a plasmonic mode with two excitonic modes, three plexitonic branches are created for a triangular CS nanoparticle in Fig.S2c. As the core size increases, the lowest branch is more affected while the middle and upper branches are less displaced. The contribution of the plasmonic mode in the formation of the lower hybrid branch is more than other hybrid branches. In other words, in

the middle and upper branches, the contribution of the excitonic modes is higher. For a specific example, the pattern of electric fields at two different plexitonic energies is shown, which is a mixture of plasmonic and excitonic electric fields. In Fig.S2d for a BL nanoparticle, from the interaction of one plasmonic peak with two excitonic peaks, three plexitonic peaks can be seen in the extinction spectra. By increasing the size of the sublayer and superlayer, the intensity of the plexitonic peaks increases and they shift to lower energies.

Extinction spectra of a cuboidal metal core, a cuboidal j- aggregate shell, a cuboidal CS and a BL nanoparticle (circular sublayer/cuboidal shell superlayer) for different structural sizes are drawn in Fig.S3. As expected, there are two plasmonic peaks in Fig.S3a due to the deviation from the circular geometry and elongation of its geometry in the x,y directions. The unclear plasmonic mode of the combination of GA and PSOA has been identified and its location is given in Fig.S12. A shift in the plasmonic peaks towards lower energies can be seen with the increase in the size of the core, and as the core enlarges, their localization increases. The plot of the electric field for the size of 30 nm at energy 2.013 eV shows that it is enhanced on the external edges of the core. Three excitonic peaks in a cuboidal j- aggregate shell nanoparticle are evident in Fig.S3b, which are red shifted with increasing hole size in the shell. For a specific example, the behavior of the electric field at two different energies is shown, a comparison between the plasmon electric fields and excitons states that excitons have less damping and while the electric field intensity of plasmons was stronger. In a cuboidal CS nanoparticle in Fig.S3c, from the interaction of two plasmonic modes of the core with three excitonic modes of the shell, five plexitonic modes can be seen. The lowest mode has a significant shift towards lower energies as the core increases, while all of them increase in intensity. For an example, at two given energies, the behavior of plexitonic electric fields is drawn, which is different from the behavior of plasmonic and excitonic electric fields. When a cuboidal j-aggregate shell is

supported on a circular metal core, from the interaction of one plasmonic mode of the core with three excitonic modes of the shell, four plexitonic modes are obtained, which are shown in Fig.S3d, and have a behavior similar to Fig.S3c.

In Fig.S4, the extinction spectra of a hexapod metal core, a hexapod j-aggregate shell, a hexapod CS and a BL nanoparticle (circular sublayer/hexapod shell superlayer) are drawn. In Fig.S4a, it is clear that with the increase in the size of the core, they have a red shift, their intensity increases and attenuation decreases. In this structure, there is a visible plasmonic peak and a hidden peak which is determined by the GA and PSOA whose location is known for a selected size in Fig.S13. The pattern of the electric field states that the vertices that are located in the direction of the incident electric field are strengthened more than other corners. There are three excitonic modes in the extinction spectra of a hexapod j-aggregate shell, which increases the intensity of the dimer peak as the hole size of the shell increases and shifts to lower energies (see Fig.S4b). The pattern of electric fields in excitonic peaks shows that hot spots are formed at vertices and corners. In a hexapod CS in Fig.S4c, the entanglement of three excitonic modes of the hexapod j-aggregate shell with two plasmonic modes of the core has formed five plexitonic branches. Broad peaks located at low energies are shifted more by changing the size of the core, while sharp peaks are shifted less in terms of energy. The behavior of electric fields indicates to the hybridization of plasmons and excitons at plexitonic energies. In Fig.S4d for a BL nanoparticle, from the interaction of a plasmonic mode from the circular core with three excitonic modes from the hexapod j-aggregate shell, four plexitonic modes can be seen, which behave similarly to Fig.S4c in different structural sizes.

For a bare heptapod metal core, a bare heptapod j-aggregate shell, a heptapod CS, and a BL nanoparticle (circular sublayer/ heptapod shell superlayer), the extinction spectra are given in Fig.S5. The results obtained in Fig.S5a show that there are two types of plasmonic peaks in the

heptapod nanocore. The first one is clearly visible, and as expected, with the increase in the size of the core, their displacement increases and they have a red shift. The second occurs in order to couple plasmons with excitons at lower energies, which is given for a 15.5 nm core in Fig.S14. Due to the presence of sharp vertices in the structure and the accumulation of more surface charges, the hot spots formed in this geometry are more. Three excitonic modes in a heptapod j-aggregate shell appear in Fig.S5b, and the dimer peaks have less displacement with increasing hole size. Similar to the electric fields in the plasmonic peaks, they are amplified at the vertices and corners of the structure. From the results obtained for a heptapod CS in Fig.S5c, it is inferred that five polariton branches are obtained from the hybridization of plasmons and excitons. The lower polariton branches are more affected than the upper ones with the increase in the core size. The pattern of electric fields in two plexitonic peaks indicates the entanglement of plasmons with excitons. From the hybridization of a plasmonic mode of the circular core with three excitonic modes of the heptapod j-aggregate shell as a BL nanoparticle in Fig.S5d, four plexitonic modes can be seen, which have the same behavior as Fig.S5c.

In Fig.S6, the extinction spectra of nanoparticles in the form of a octapod metal core, a octapod j-aggregate shell, a octapod CS and a BL (circular sublayer/ octapod shell superlayer) in different structural sizes as a function of photon energy are drawn. As it is clear from Fig.S6a, the visible plasmonic peaks in this nanostructure shift to lower energies with the increase in size, and their localization increases. Although there is also a hidden plasmonic peak that was determined by the GA+PSOA, its location is indicated in Fig.S15 for a given size. The electric field plot showed that more vertices were heated due to being placed in the direction of the incident electric field. In Fig.S6b, for a octapod j-aggregate shell, there are three excitonic modes which are sharper than the plasmonic modes and have less displacement as the hole size increases. The behavior of their electric field showed that its value is enhanced in the corners

located in the direction of the incident electric field. For a octapod CS in Fig.S6c, five plexitonic modes are seen due to the hybridization of plasmons and excitons. The sharp polariton peaks are less affected by the increase in the size of the core than the broad peaks in terms of photon energy. The pattern of electric fields of two polaritonic peaks indicates that an entanglement has occurred between the component modes of a plexitonic system. In a BL nanoparticle in Fig.S6d, four plexitonic modes can be seen from the entanglement of a plasmonic mode of the circular core with three excitonic modes of the octapod j-aggregate shell, which have the same behavior as Fig.S6c. It is necessary to mention that by adding vertices to the structure of Fig.S6, its optical behavior becomes closer to Fig.3.

Extinction spectra of a starfish 4-arms metal core, a starfish 4-arms j-aggregate shell, a starfish 4-arms CS nanoparticle, and a BL nanoparticle (circular sublayer/ starfish 4-arms shell) in Fig. S7 are given as a function of photon energy at different structural sizes. In Fig.S7a, it is clear that the plasmonic modes were located at low energies due to the small surface area. As the core size increases, they shift to lower energies. The pattern of the electric field shows that its value is strengthened in the corners of the structure. In this structure, there is an obvious plasmonic mode and a hidden plasmonic mode, whose location is determined by the GA+PSOA in Fig.S16 for a selected size. In Fig.S7b, three excitonic modes are considered for a starfish 4-arms j-aggregate shell, and the position of the dimer peaks shifts less with increasing shell size and their intensity increases. The intensity of electric fields and extinction spectra in this structure is lower than in the metal core. From the interaction of two plasmonic modes with three excitonic modes in CS nanoparticle, five plexitonic modes can be seen in Fig.S7c. The hybrid modes located at low energies have more displacement than other modes with increasing core size. The behavior of electric fields in a inset plot shows that plasmonic modes are mixed with excitonic modes. From the entanglement of a plasmonic mode from the circular core with

three excitonic modes from the starfish 4-arms j-aggregate shell in Fig.S7d, four plexitonic modes can be observed, which have the same behavior as Fig.S7c.

In Fig.S8, the extinction spectra of a starfish 6-arms metal core, a starfish 6-arms j-aggregate shell, a starfish 6-arms CS nanoparticle, and a BL nanoparticle (circular sublayer/ starfish 6-arms shell) are given. In Fig.S8a, for a starfish 6-arms metal core, there is a plasmonic peak that is red shifted with increasing core size. The hot spots are formed at the four vertices of this structure due to being located in the direction of the incident electric field. In Fig.S8b, for a starfish 6-arms j-aggregate shell, two excitonic modes occur, and their intensity increases with the increase of the hole size. The behavior of electric fields shows that its value is enhanced at the corners located in the direction of the applied electric field. From the interaction of a plasmon mode with two excitonic modes in a starfish 6-arms CS nanoparticle in Fig.S8c, three plexitonic modes are formed, the narrower peaks of which are less affected by increasing the size of the core. The behavior of the electric field in the plexitonic peaks indicates the hybridization of plasmon with excitons. In Fig.S8d, for a BL nanoparticle, three plexitonic modes are formed, which is caused by the hybridization of one plasmonic mode from the circular sublayer and two excitonic modes from the superlayer shell. And these modes, by changing the dimensions of the core and hole of shell, have the same behavior as Figs.S8c& S8b, respectively. We repeated the previous calculations in Fig.S9, in this way, the core is considered as a starfish 7-arms nanoparticle(Fig.S9a), and the shell as a starfish 7-arms j-aggregate shell (Fig.S9b), the CS as a starfish 7-arms CS nanoparticle(Fig.S9c) and the BL as a BL nanoparticle (circular sublayer/ starfish 7-arms shell superlayer)(Fig.S9d). Here also, the intensity behavior of extinction spectra and electric fields in the core, shell, CS and BL is similar to Fig.S8, with the difference that there are three excitonic modes in the shell, four plexitonic modes in the CS, and three plexitonic modes in the BL.

Extinction spectra of an elliptical CS nanoparticle, a BL nanoparticle (circular sublayer/elliptical shell superlayer) and their components as a function of photon energy in a selected size are shown in Figs.S10a and S10b, respectively. In Fig.S10a, there are 6 spectral peaks for the elliptical CS, the broadest of which is at the energy of 1.94 eV and the narrowest one is at the energy of 2.13 eV. The plasmonic mode of the core corresponds to the excitonic mode of the shell at the energy of 2.11 eV. For the BL nanoparticle in Fig.S10b, 7 spectral peaks have been introduced, the widest and narrowest of which occurred at energies of 2.02 and 2.17 eV, respectively. The plasmonic mode of the superlayer (2.14 eV) is located very close to the j-band (X3) of the sublayer. The Level splitting energy (Ω_{LS}), the coupling strength (g), the damping of plasmon and excitons (Γ_p, Γ_x) as a function of detuning for both plexcitonic nanoparticles are given in in Figs.S10c and S10d. In Fig.S10c, the dominant regime in the plasmon-exciton interaction was of the SCR. At zero detuning, the Rabi splitting energy of 194 meV can be obtained for this nanostructure. In Fig.S10d for the bilayer nanoparticle, most couplings were of intermediate type. The Rabi splitting energy obtained here is approximately 170 meV. The weight percentages of the Hopfield coefficients of plasmon and excitonic modes in the formation of plexcitonic hybrid modes for circular CS and BL nanoparticles are drawn in Figs.S10e and S10f. From Fig.S10e, it is clear that the plasmonic mode contributed to the formation of all hybrid modes, the highest and lowest of which was in PX1 and PX3, respectively. The highest contribution of the first to third excitonic modes occurred in the hybrid modes of PX2 to PX4 respectively, and the major contribution of the 4th and 5th excitonic modes was in the formation of the 5th plexcitonic energy. PX3 is a pseudo-plexciton because it is formed only from excitons. From Fig.S10f, it is clear that all the first to fifth excitonic modes and the plasmonic mode participated in the formation of the plexcitonic energies of PX1 to PX6. While the excitonic mode X6 only contributed 100% to the 7th spectral peak. Therefore,

PX7 is not a real plexitonic peak (see Fig.S10b). As can be deduced from Fig.S10d, its coupling rate was very weak at about 4 meV. Here, the high value of $\Omega_{LS} = 169$ meV is due to the difference in the individual plasmonic and sixth excitonic levels.

In Fig.S11a, the results of the extinction spectra of a triangular CS nanoparticle and its components are given as a function of photon energy. Here, 9 spectral peaks have appeared in the CS nanoparticle, the narrowest and broadest of which are located at the energies of 2.12 and 1.72 eV, respectively. The plasmonic mode is outside of the exciton modes, and in order to couple with excitons, the size of the core must be reduced. On the other hand, by reducing the size of the core, the intensity of the plasmon peak decreases, which does not have an effective electric field for the coupling with excitons. Also, in Fig.S11b for the BL nanoparticle (circular sublayer/ triangular shell superlayer) there are 7 spectral peaks whose energies are between 1.99 and 2.20 eV. The results obtained in Fig.S11c showed that the coupling strength of mode X1 with plasmon is zero. The value of Ω_{LS} here is caused by the difference in plasmonic and excitonic levels. With these conditions, it is not possible to introduce a Rabi splitting energy in this nanostructure. In Fig.S11d for the BL nanoparticle, a strong coupling regime has occurred between the plasmonic mode and the third excitonic mode. By choosing a suitable size for the metal sublayer, in this case, a Rabi splitting energy of about 79 meV can be achieved. It can be seen from Fig.S11e that the plasmonic mode has the largest contribution in the formation of the PX1 hybrid mode and excitonic modes are effective in the formation of other hybrid modes. The second spectral peak consists only of the first excitonic mode, so it is not a real plexitonic mode (see Fig.S11a). Fig.S11f shows that the plasmonic mode contributes more to the formation of PX3 and PX6 hybrid modes. The contribution of the plasmonic mode in the formation of the spectral peaks of PX1, PX2 and PX7 is very small, and they consist only of the excitonic modes X1, X2 and X6, respectively. Therefore, they are not real plexitons and we

excluded them from the hybrid modes (see Fig.S11b). Here, PX3 in CS and PX4 in BL are pseudo-plexitons.

In Fig.S12a, for a cuboidal CS, 7 spectral peaks can be observed in the extinction spectra, which are obtained from the hybridization of two plasmonic modes from the core and 5 excitonic modes from the shell. The narrowest and broadest spectral peaks occurred at energies of 2.14 and 1.90 eV, respectively. The main plasmonic mode (P2) corresponds to the narrow excitonic mode (j-band). The first plasmonic mode (P1) was obtained by combining the GA with the PSOA in order to calculate the coupling strengths in the off-diagonal elements of the Hamiltonian in Eq.3. In Fig.S12b, for a BL nanoparticle (circular sublayer/ cuboidal shell superlayer), 6 spectral peaks can be seen, which are the result of the interaction of a plasmonic mode from the sublayer with 5 excitonic modes from the superlayer. The energy of these spectral peaks is between 1.97 and 2.24 eV. In Fig.S12c, it is obvious that all coupling rates are strong. The values of the level splitting energy are related to the main plasmon. At zero detuning in this nanostructure, the Rabi splitting energy of 125 meV can be obtained. In Fig.S12d for a BL nanoparticle, two types of strong and intermediate coupling regimes were found. The strongest one was obtained from the interaction of the third exciton mode(X3) with the plasmonic mode. Here, at zero detuning, the Rabi splitting energy can be reached to 171 meV. In Fig.S12e, it can be seen that the main plasmonic mode (P2) contributes to the formation of all plexitonic modes, while the first plasmonic mode (P1) has the greatest effect on plexitonic modes PX2 and PX3. Excitonic modes X1 to X5 have had the largest share in hybrid modes PX1, PX4, PX5, PX6 and PX6, respectively. It is obvious in Fig.S12f that the plasmonic mode contributed to the formation of all plexitonic modes. Excitonic modes X1 to X5 had the most effect on plexitonic modes PX1, PX2, PX4, PX5 and PX6, respectively.

Extinction spectra of hexapod CS and BL nanoparticles (circular sublayer/hexapod shell superlayer) and their components are given in Figs.S13a and S13b . From the hybridization of two plasmonic modes from the core with six excitonic modes from the shell, 8 plexitonic modes are formed in Fig.S13a. The narrowest plexitonic mode occurred at the energy of 2.14 eV. The main plasmonic mode of the core is located close to the excitonic mode X3 (j- band). Based on our calculations for this nanostructure, both plasmonic modes are effective in the formation of plexitonic modes.As can be seen from Fig.S13b, from the interaction of one plasmonic mode from the sublayer with six excitonic modes from the superlayer, seven excitonic modes are observed in the extinction spectra for a BL nanoparticle, whose energy is distributed between 1.97 and 2.23 eV. Here, by choosing a suitable size for the sublayer, the plasmonic mode is set between the excitonic modes.Two types of strong and intermediate coupling regimes were observed for the CS nanoparticle in Fig.S13c, and most of them were of SCR. By placing the main plasmon mode between X3 and X4 excitonic modes, the Rabi splitting energy can be adjusted between 93 and 131 meV. For the BL nanoparticle in Fig.S13d, three types of coupling SCR ,ICR,and WCR were found, the strongest of which occurred from the interaction of the third excitonic mode with the plasmonic mode. Due to the closeness of the plasmonic mode to the j-band, the energy of the Rabi splitting can be obtained at about 129 meV.It can be seen from the Hopfield coefficients in Fig.S13e that both plasmons are effective in the formation of all hybrid modes. As it is known, all excitonic modes contribute to the formation of plexitonic branches and none of them can be ignored. It is clear from the Fig.S13f that the plasmonic mode has the largest contribution in the formation of PX3 and PX7. With the increase of plexiton energy, the contribution of X1 excitonic mode decreased. Excitonic modes X2 to X6 had the largest share in plexitonic modes PX2, PX4, PX5, PX4 and PX6, respectively.

Fig.S14a shows that for a heptapod CS nanoparticle, there are 8 plexitonic branches, which consists of the hybridization of two plasmonic modes of the core and six excitonic modes of the shell. The longest plexitonic branch (PX5) occurred between the narrow excitonic modes X3 and X4 and near the main plasmonic mode(P2). For a BL nanoparticle (circular sublayer/heptapod shell superlayer) in Fig.S14b, there are 6 plexitonic branches that are the hybridization of a plasmonic mode from the sublayer and 5 excitonic modes from the superlayer. The plasmon mode is very close to the sharp excitonic mode (X3). The energy of excitonic branches is distributed between 1.98 and 2.24 eV. From Fig. S14c, it was found that there are two regimes of strong and intermediate coupling in plasmo-exciton interactions. Due to the fact that the main plasmonic mode is between the third and fourth excitonic modes, the Rabi splitting energy can be set between 123 and 184 meV. In Fig.14Sd for the BL nanoparticle, there are three types of coupling SCR,ICR, and WCR, the strongest of which was $g = 68$ meV, which was formed from the coupling of the j- band with the plasmonic band. It is possible to adjust the Rabi splitting energy values from 101 to 111 meV due to the placement of the plasmonic band between the third and fourth excitonic bands. The results obtained for Hopfield coefficients in Fig.S14e showed that plasmonic and excitonic modes were involved in the formation of all plexitonic branches. It is clear from the Fig.S14f that the plasmonic mode contributes to the formation of all the plexitonic modes. The excitonic modes X1 and X5 have decreased and increased respectively with the increase of the plexiton energy. Excitonic modes X2 to X4 have contributed the most in the formation of plexitonic modes PX2, PX4 and PX4, respectively.

In Fig.S15a, for a hexapod CS nanoparticle, 8 plexitonic modes were observed, which is the result of the hybridization of 2 plasmonic modes from the core and 6 excitonic modes from the shell, and the energy of the plexcitonic modes is in the range of 1.90 to 2.40 eV. The main plasmonic mode is located between narrow excitonic modes X3 and X4. In Fig.S15b, for a BL

nanoparticle (circular sublayer/hexapod shell superlayer), 6 plexitonic modes were observed, which was the result of the interaction of a plasmonic mode from the sublayer with 5 excitonic modes from the superlayer. The plasmonic mode was located between the excitonic modes and close to the X3 excitonic mode. Two types of strong and intermediate coupling were found in Fig.S15c, and the majority of them were of SCR type. Due to the placement of the main plasmonic mode between the sharp X3 and X4 excitonic modes, the Rabi splitting energy values can be tuned between 122 and 133 meV. In Fig.S15d for a BL nanoparticle, two types of strong and intermediate coupling regimes were found, the strongest of which was the interaction of the plasmonic mode with the exciton X3 mode with $g = 78$ meV. The value of the Rabi splitting energy can be changed between the level splitting energy values from 104 to 123 meV. From Fig.S15e, it was observed that all plasmonic and excitonic modes were effective in the formation of all plexitonic modes. It is also clear from Fig.S15f that the plasmonic mode contributed to the formation of all the hybrid modes of a BL nanoparticle. Here, the X1 and X5 modes decreased and increased, respectively, with the increase of the plexiton energy. The X2 to X4 modes had the largest contribution in the formation of the PX2, PX3 and PX3 hybrid branches, respectively.

In Figs.S16a and S16b, the extinction spectra for starfish 4-arms CS and BL (circular sublayer/starfish 4-arms shell superlayer) nanoparticles and their components as a function of photon energy are shown. For the CS nanoparticle in Fig.S16a, 8 spectral peaks were observed in the extinction spectra. Both plasmonic modes are located outside the excitonic modes, so the possibility of forming real plexitons for this nanostructure is low. Here, P1 mode due to its sharpness and high extinction intensity was considered as the main plasmon mode. In Fig.S16b, 7 plexitonic branches due to hybridization of one plasmon mode from the sublayer and 6 excitonic modes from the superlayer were observed. Due to the thinness of the shell in the

superlayer, the intensity of excitonic modes in the extinction spectra is low. The plasmonic mode is close to the excitonic mode. In Fig.S16c, three types of SCR, ICR, and WCR were observed. Weak couplings included very weak X2 to X4 interactions with the plasmonic (P1) mode. The intermediate coupling was due to X1 interaction with the main plasmonic mode. Strong couplings include X5 and X6 interactions with the P1 mode. It is not possible to determine the Rabi splitting energy due to the exclusion of the plasmonic mode from the excitonic modes in this nanostructure with the selected sizes. In Fig.S16d for the BL nanoparticle, three types of strong, intermediate, and weak coupling were observed, most of which are intermediate. Due to the placement of the plasmonic mode between the X4 and X5 modes, the Rabi splitting energy can be tuned between 37 and 61 meV. The results obtained for the Hopfield coefficients in Fig.S16e showed that the PX1 and PX2 branches are pseudo-plexitons. Because the plasmonic modes contributed the most in the formation of these hybrid branches. The spectral peaks PX3-PX6 in the extinction spectra are not real plexitons because they exactly correspond to the corresponding excitonic modes. So we removed them from the CS extinction spectra. The contribution of plasmon in the formation of PX7 and PX8 hybrid branches was about 3%. It is clear from Fig.S16f that excitonic modes and plasmonic modes contributed to the formation of all plexitonic modes. Although the PX6 hybrid mode is a pseudo-plexiton mode because most of the excitons contributed to its formation.

In Fig.S17a, in the extinction spectra of a starfish 6-arms CS nanoparticle, 8 spectral peaks were observed, whose energies are between 1.92 and 2.35 eV. The majority of excitonic modes for the chosen size of the core is located outside the plasmonic mode. In Fig.S17b, for a BL nanoparticle (circular sublayer/ starfish 6-arms shell superlayer), there are 7 plexitonic modes, which are caused by the hybridization of a plasmonic mode with six excitonic modes. The plasmonic mode almost coincides with the X4 mode. The results obtained in Fig.S17c showed

that the X1 and X2 modes do not interact with the plasmonic mode. Other couplings were of intermediate and strong type. With the structural parameters chosen for this CS nanoparticle, it is not possible to calculate the Rabi splitting energy. For the BL nanoparticle in Fig.17Sd, the coupling rates were of strong, intermediate, and weak types. By adjusting the plasmonic mode between the third and fourth excitonic modes, values of Rabi splitting energy of 25 to 94 meV can be reached. Fig.S17e shows that PX2 and PX3 are not real plexcitons and they are 100% of X1 and X2 excitons, respectively. Also, PX5 is a pseudo-plexciton because excitons have a major contribution to its formation. Fig.S17f shows that plasmon and excitons contributed to the formation of all plexciton branches.

In Figs.S18a and S18b, the extinction spectra for starfish 7-arms CS and BL (circular sublayer/ starfish 7-arms shell superlayer) nanoparticles and their components as a function of photon energy are given. In Fig.S18a for the CS nanoparticle, 8 spectral peaks were observed in the extinction spectra, whose energies were between 1.62 and 2.34 eV. The plasmonic mode is considered outside the excitonic modes. In Fig.S17b for the BL nanoparticle, there are 6 plexcitonic modes that result from the hybridization of a plasmonic mode with 5 excitonic modes. Here, the plasmonic mode coincides with the X4 mode. In Fig.S18c, the coupling rates were of strong and medium type. With the structural parameters chosen for the starfish 7-arms CS nanoparticle, the Rabi splitting energy cannot be determined. In Fig.S18d, the coupling rates were strong, intermediate, and weak. At zero detuning, the Rabi splitting energy can reach to 80 meV. The results of Hopfield coefficients for the CS nanoparticle in Fig.S18e showed that PX2 and PX3 are pseudo-plexcitons. Because they are mostly composed of excitons. It is also clear in Fig.S18f that plasmon and excitons contributed to the formation of all plexcitonic modes.

In Fig.S19, the transition dipole moment and charge displacement of excitons of shell and superlayer in CS and BL for elliptical, triangular, and cuboidal nanoparticles as a function of exciton energy are shown. In Fig.S19a, it is clear that the strongest transition dipole moment is formed in third excitonic mode. Its values for elliptical shell and superlayer were 253 and 183 Debye. The corresponding values of the charge displacement were 5.3 and 3.8 nm. In Fig.S19b, it is clear from μ_j and d_j results for triangular shell and superlayer nanoparticles that their values have increased with the increase in the energy of excitonic modes up to the third excitonic mode. The largest μ_j occurred in X3 mode, which were 150 and 126 D, respectively. The charge displacements of them were 3.1 and 2.6 nm. In Fig.S19c, for cuboidal shell and superlayer nanoparticles, the third excitonic mode has the largest μ_j and d_j . These quantities had values of 262 D and 5.5 nm for the cuboidal shell and values of 190 D and 4.0 nm for the cuboidal shell superlayer. The same trend was observed in Figs.S20a-S20c for pentapod to hexapod shell and superlayer nanoparticles. The largest values of μ_j and d_j were for them respectively, 192 D and 4.0 nm, 148 D and 3.1 nm; 142 D and 3.0 nm, 141 D and 2.9 nm; 197 D and 4.1 nm; 165 D and 3.5 nm. The same quantities were followed in starfish shell and superlayer nanoparticles in Fig.S21. It is clear from the obtained results of μ_j and d_j in Fig.S21a for starfish 4-arms shell and superlayer nanoparticles, the third excitonic mode has the highest values. Their values were respectively, 139 D and 2.9 nm, 77 D and 1.6 nm. In Figs.S21b and S21c for starfish 4- and 6-arms shell nanoparticles, the X4 mode had the highest values μ_j and d_j . They were respectively, 98 D and 2.1 nm, 120 D and 2.5 nm. Here, for starfish 4- and 6-arms superlayer shell nanoparticles, their values were respectively, 79 D and 1.7 nm, 77 D and 1.6 nm.

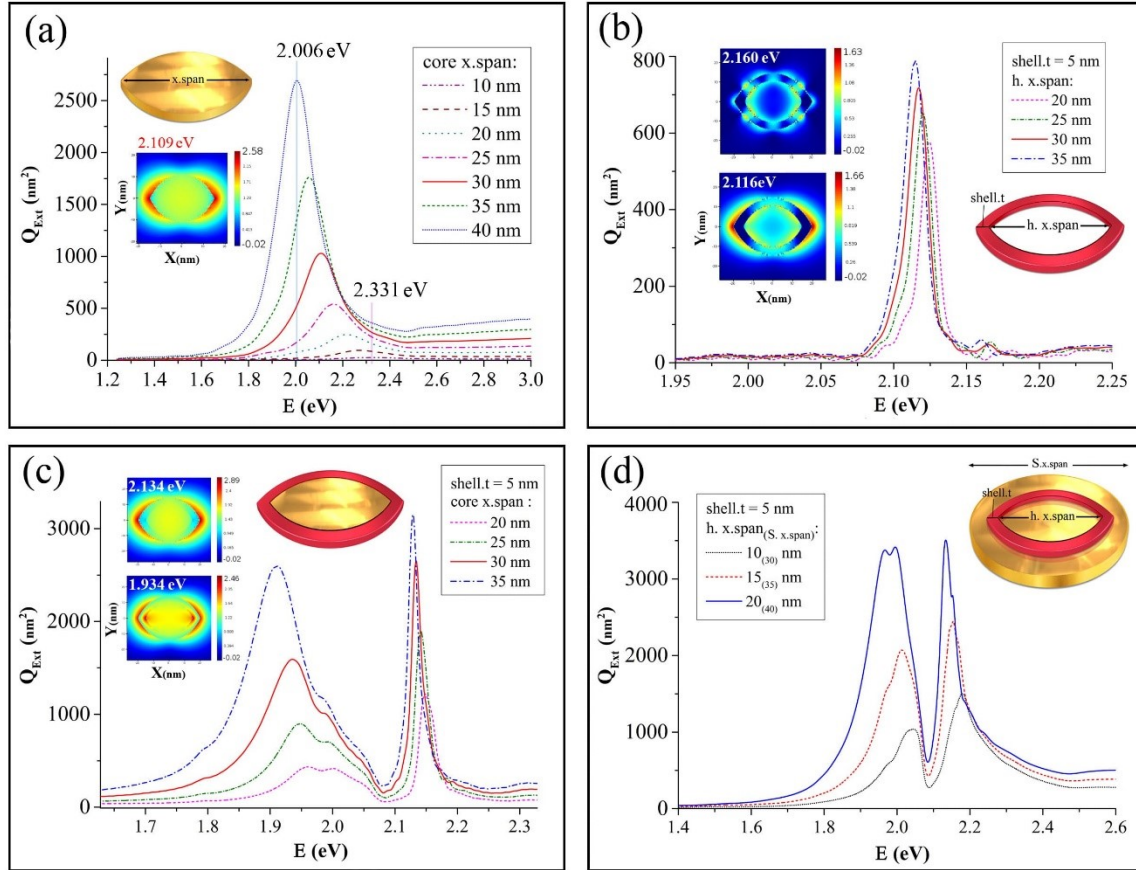


Fig.S1. Extinction spectra of elliptical curved supershape nanoparticle as a function of photon energy. (a) different x-spans of the bare metal core, (b) different x-spans of the air hole with a j-aggregate bare shell thickness of 5 nm, (c) CS nanoparticle at different x-spans of the metal core with a shell thickness of 5 nm, (d) BL nanoparticle at different x-spans of the metal sublayer and the air hole j-aggregate superlayer with shell thickness of 5 nm. The inset plots in a-c refer to depiction $\text{Log} |E|^2$ at the energies listed above them for the solid line in the ligands.

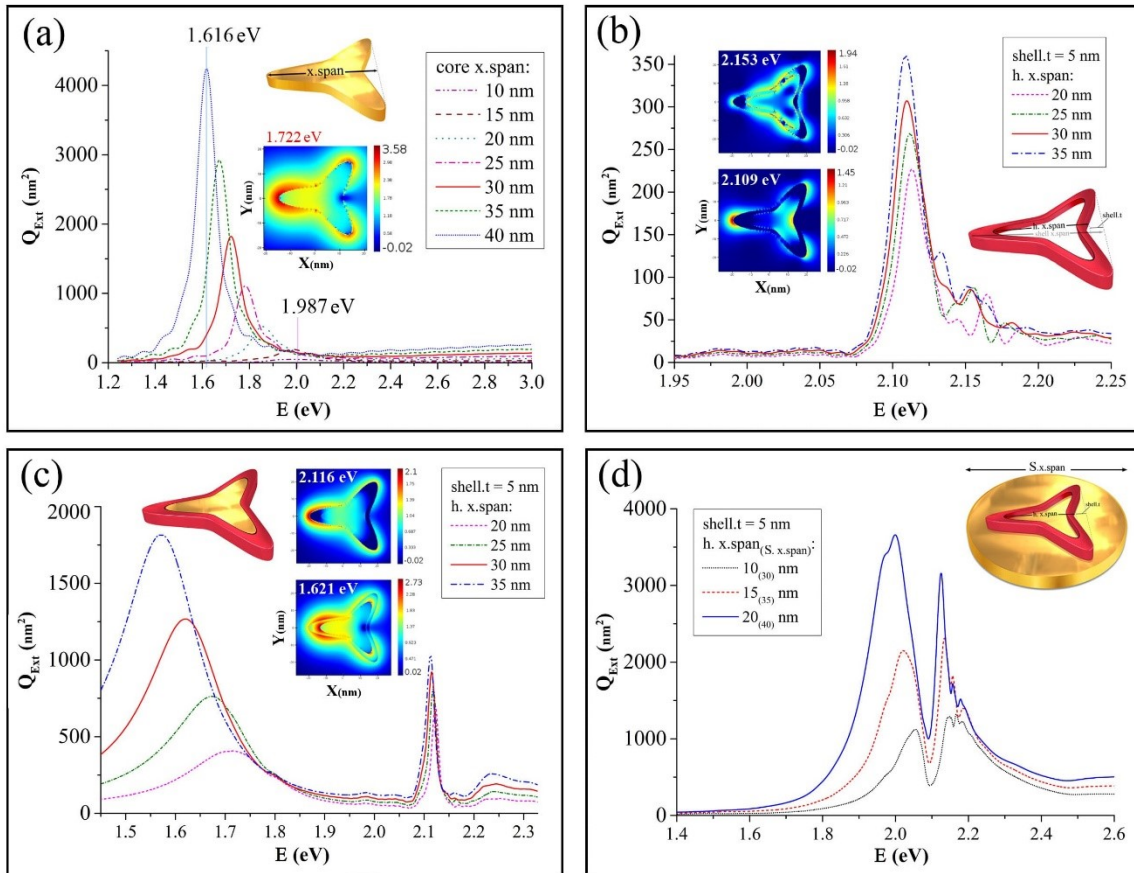


Fig.S2. Same as Fig. S1, except that the extinction spectra was calculated for triangular curved supershape nanoparticle.

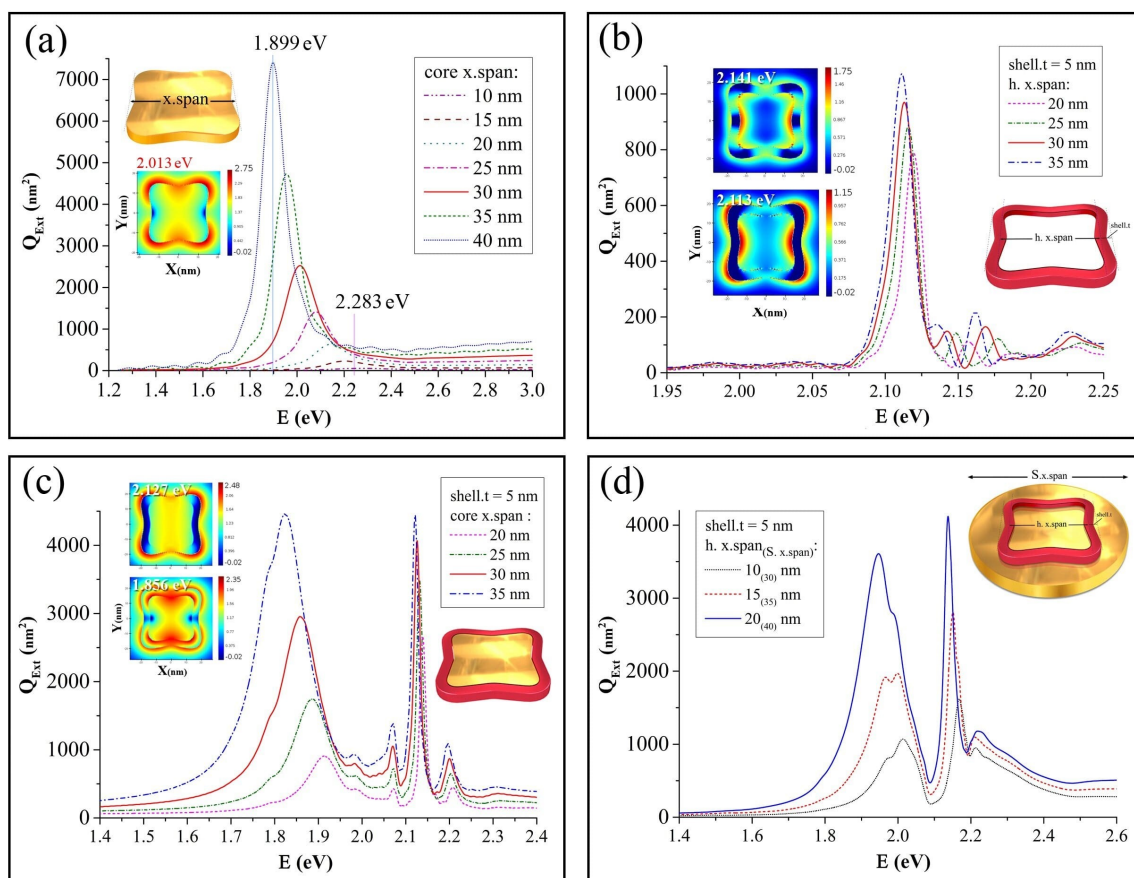


Fig.S3. Same as Fig. S1, except that the extinction spectra was calculated for cuboidal curved supershape nanoparticle.

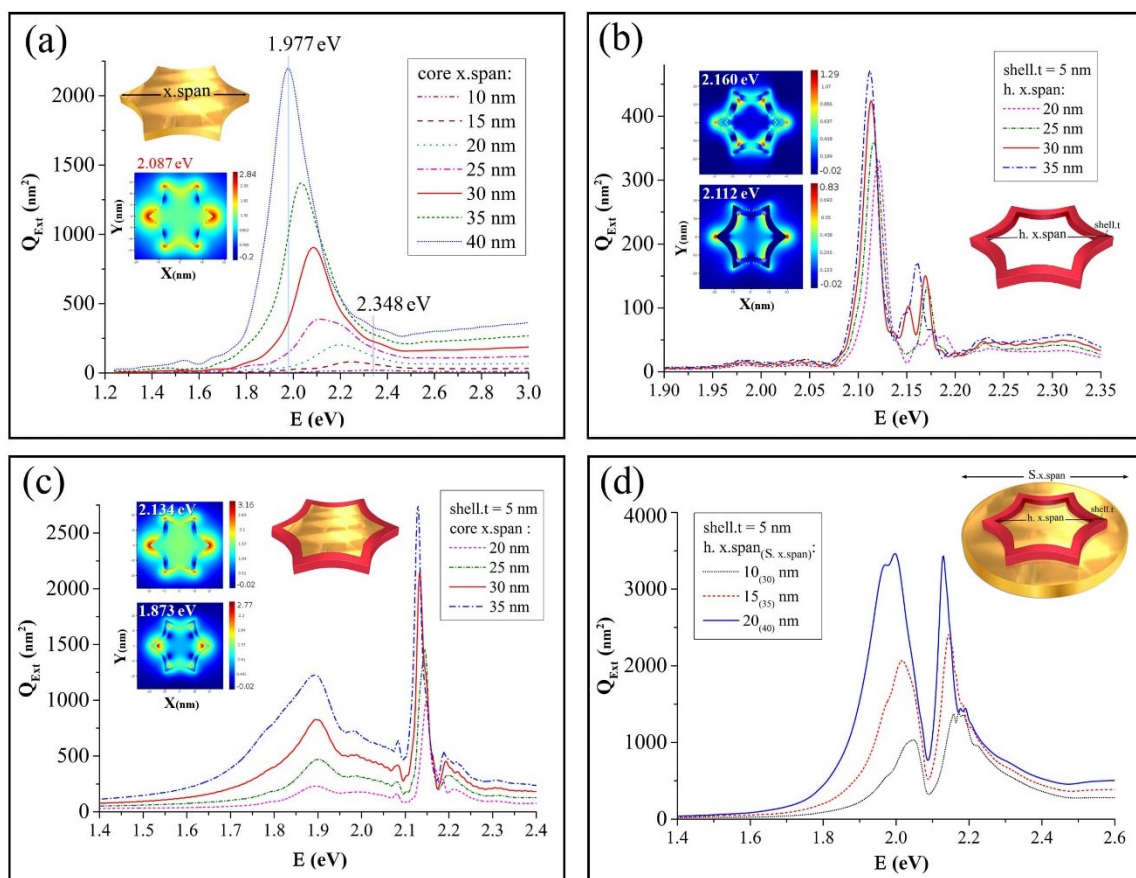


Fig.S4. Same as Fig. S1, except that the extinction spectra was calculated for hexapod supershape nanoparticle.

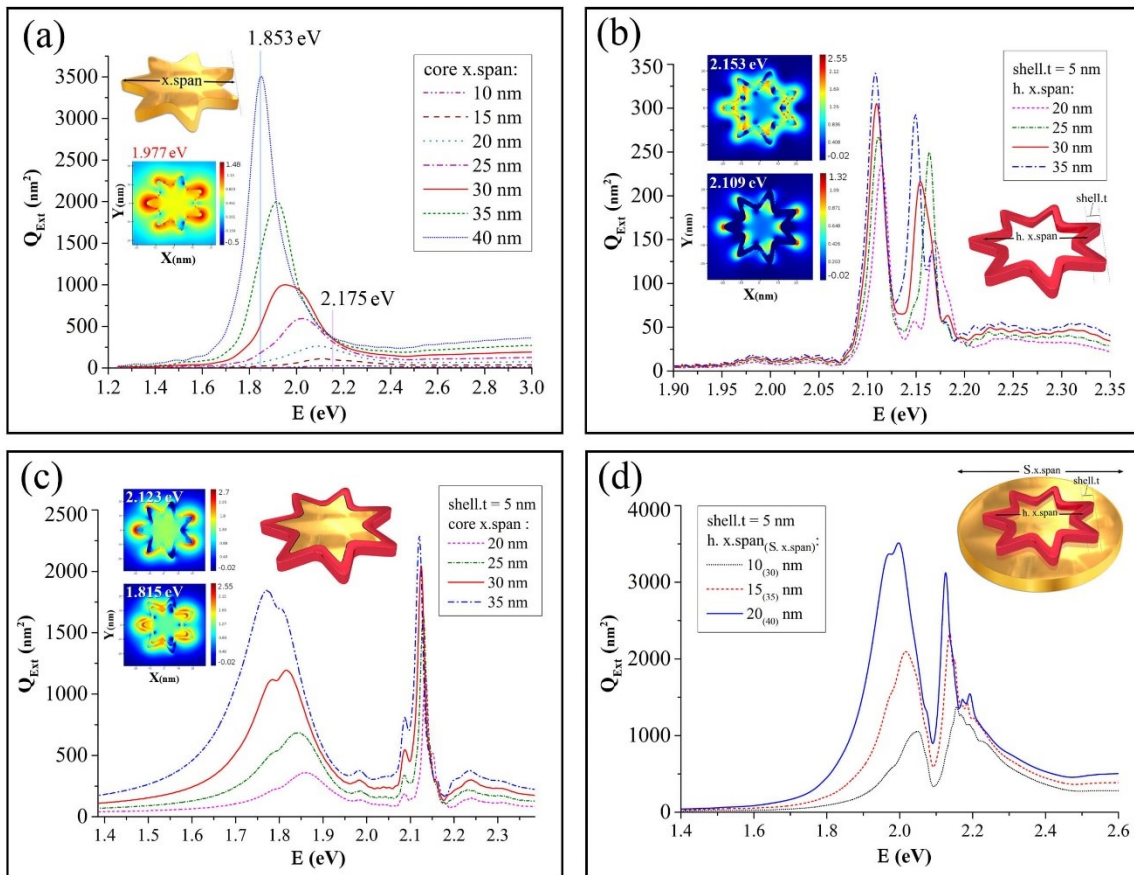


Fig.S5. Same as Fig. S1, except that the extinction spectra was calculated for heptapod supershape nanoparticle.

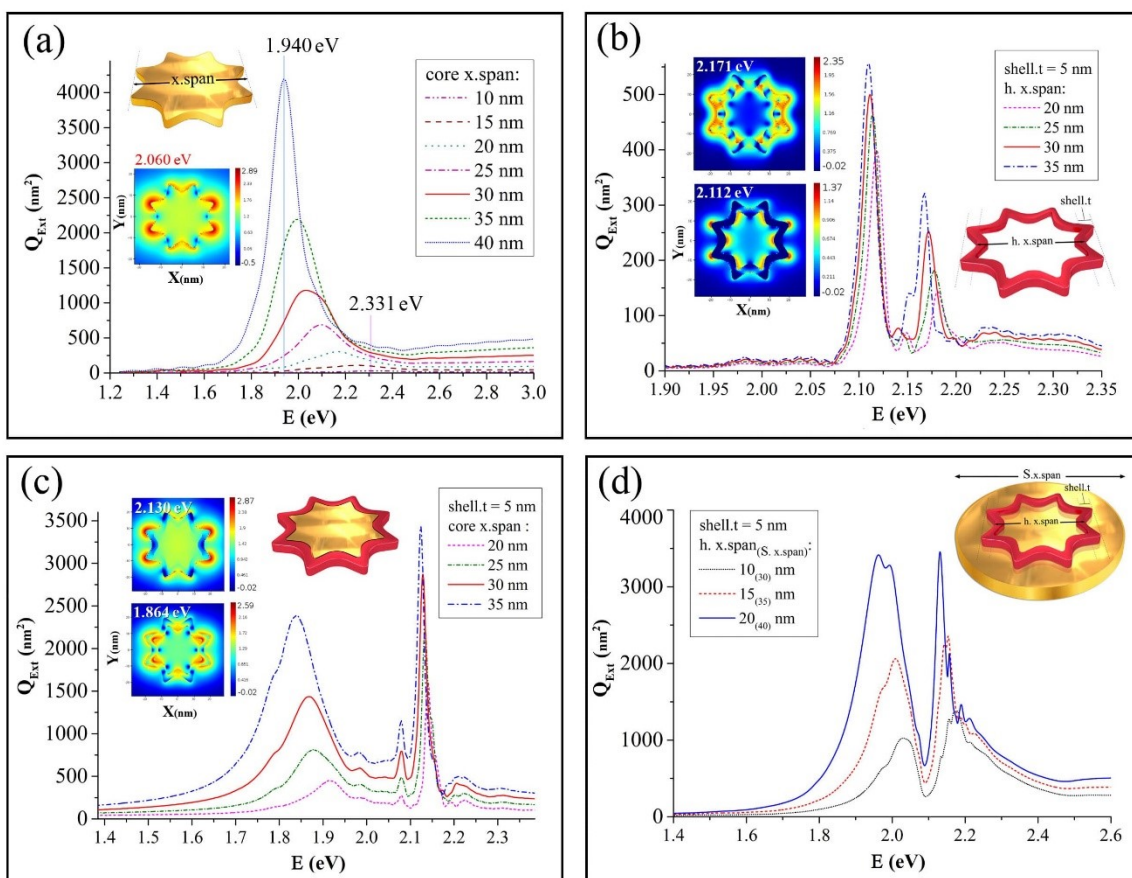


Fig.S6. Same as Fig. S1, except that the extinction spectra was calculated for octapod supershape nanoparticle.

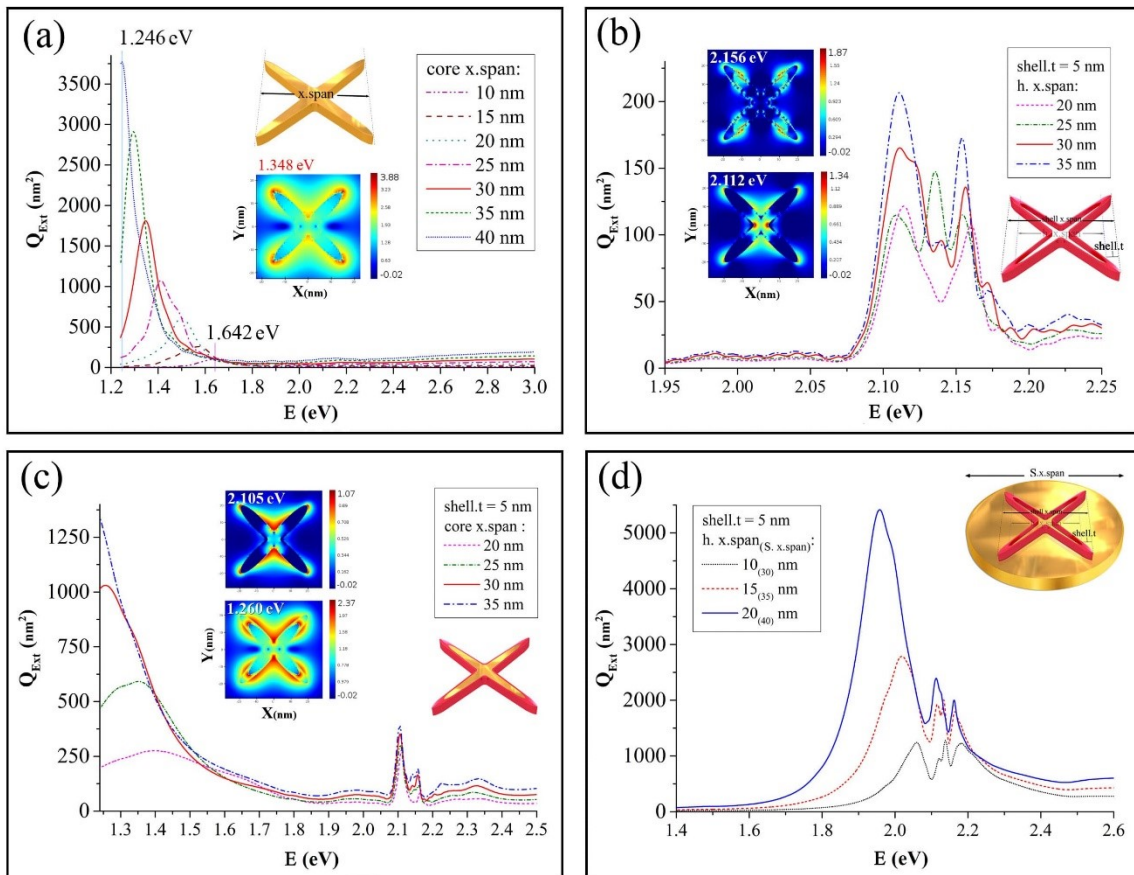


Fig.S7. Same as Fig. S1, except that the extinction spectra was depicted for 4-arms starfish supershape nanoparticle.

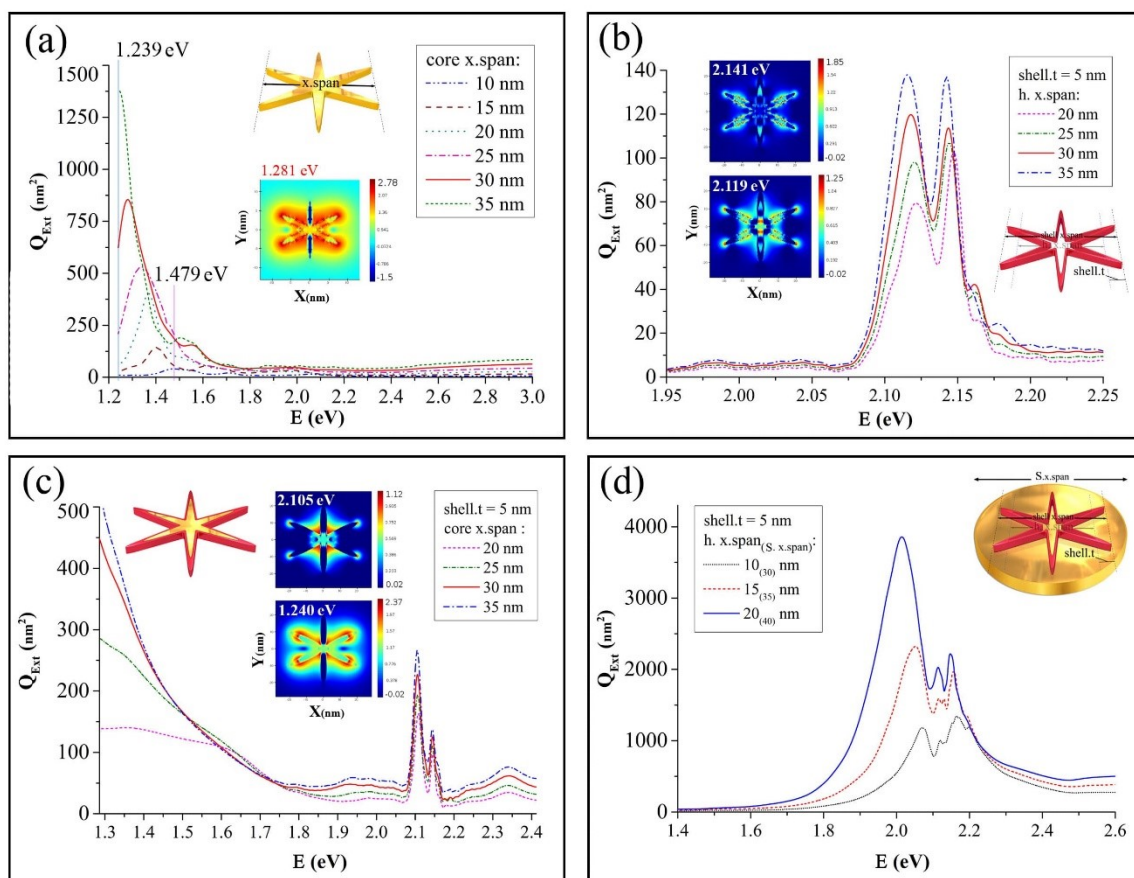


Fig.S8. Same as Fig. S1, except that the extinction spectra was depicted for 6-arms starfish supershape nanoparticle.

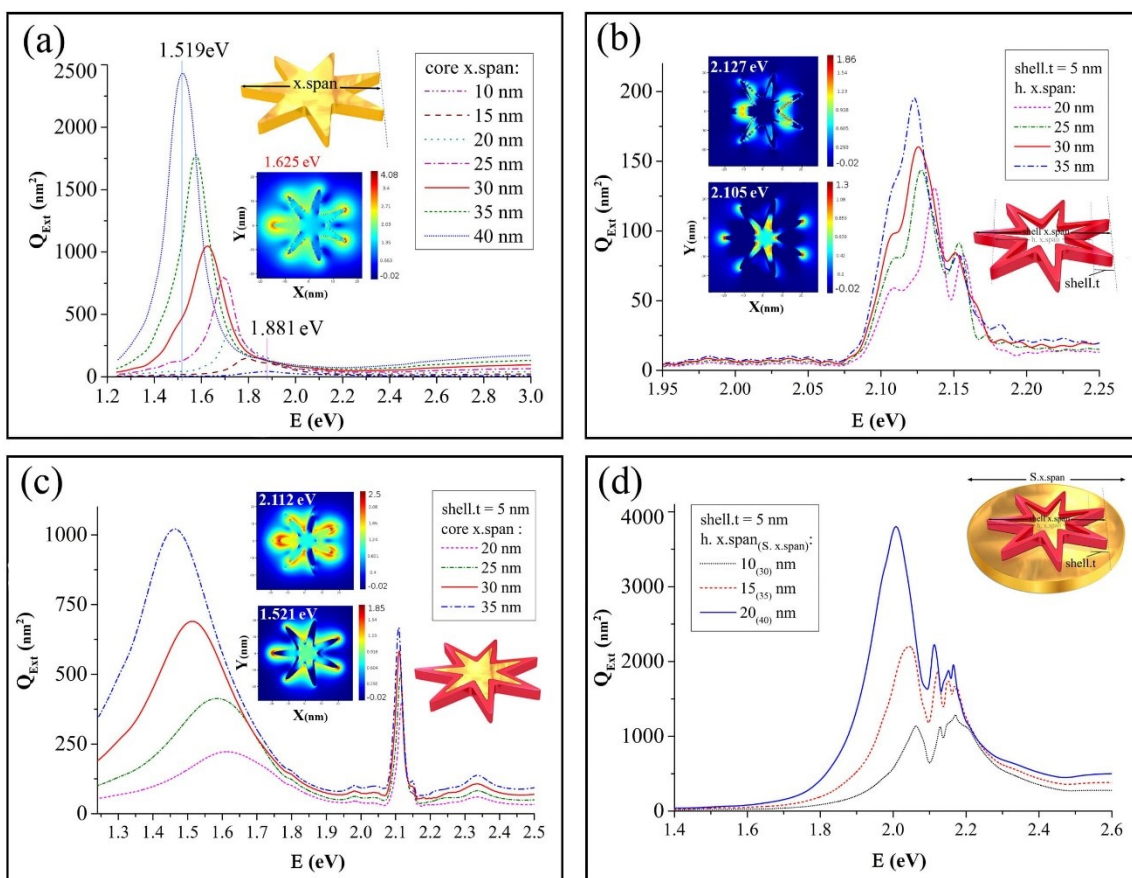


Fig.S9. Same as Fig. S1, except that the extinction spectra was depicted for 7-arms starfish supershape nanoparticle.

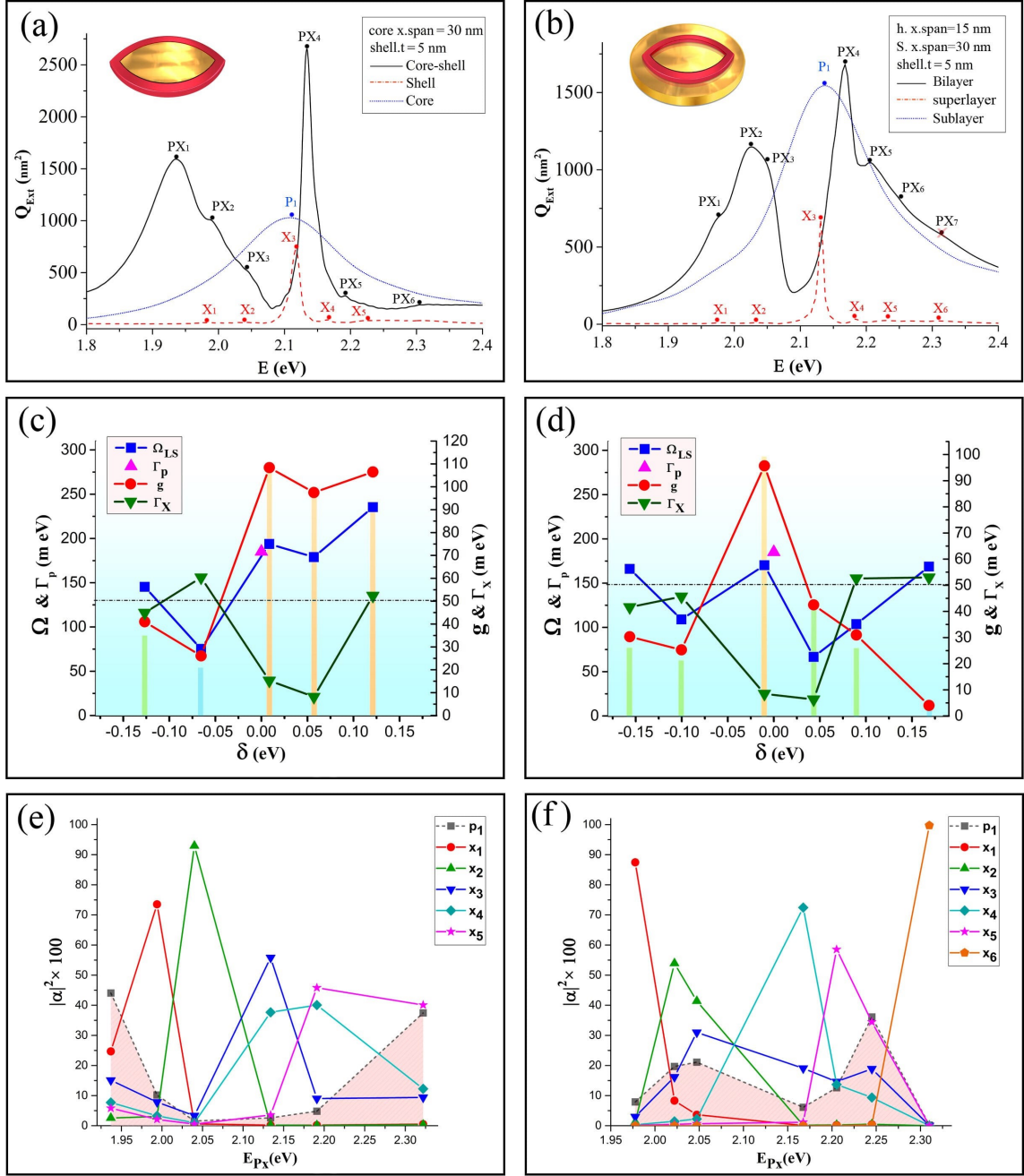


Fig.S10. (a, b) Extinction spectra as a function of photon energy for CS , BL elliptical curved supershape nanoparticles and components, (c, d) Rabi splitting energy (Ω), coupling strength (g), damping of plasmons and excitons (Γ_p, Γ_x) as a function of detuning energy ($\delta=E_p-E_x$), (e, f) weighting percent of Hopfield coefficients for plasmons and excitons as a function of plexciton energy for formation plexciton hybrid modes. The resonance peaks of plasmons (P), excitons(X), and plexcitons (PX) are marked on the plots (a, b) and they are arranged from left to right. The vertical bars in plots c&d were determined from $(4g g_0 / (\Gamma_p + \Gamma_x))$ and the horizontal line indicates $g_0 = 50 meV$.

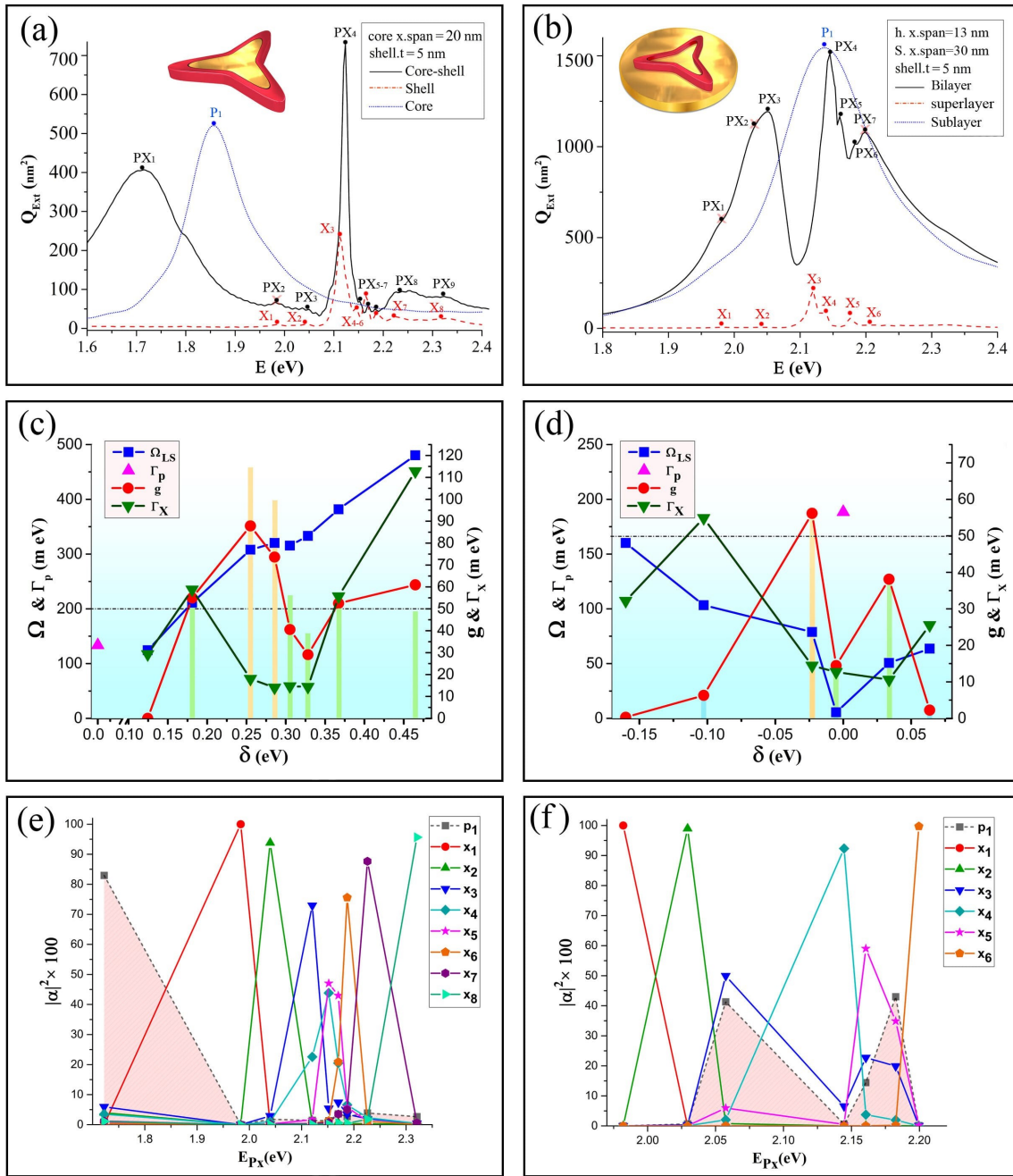


Fig.S11. Same as Fig. S10, except that the extinction spectra was calculated for triangular curved supershape nanoparticle.

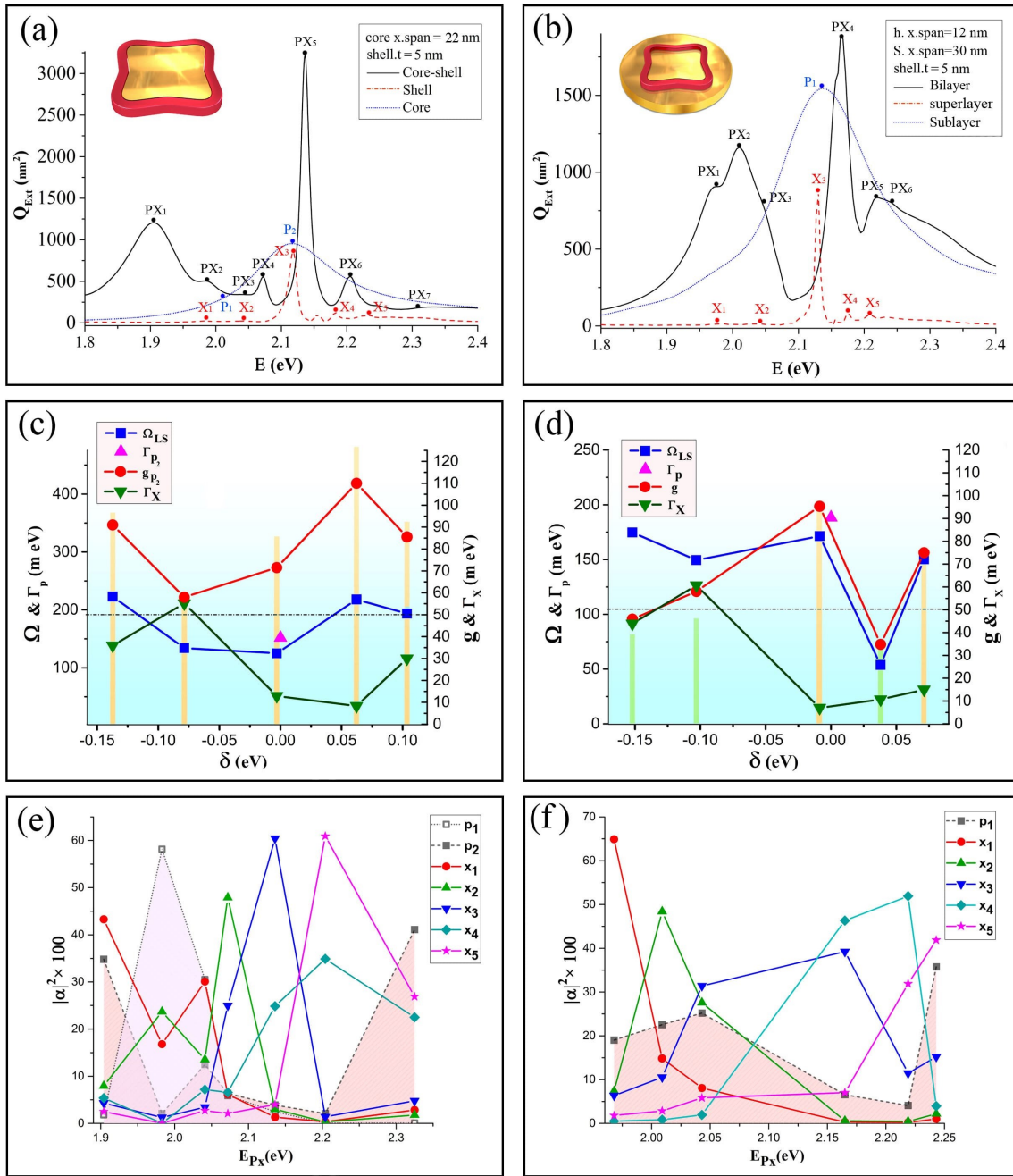


Fig.S12. Same as Fig. S10, except that the extinction spectra was calculated for cuboidal curved supershape nanoparticle.

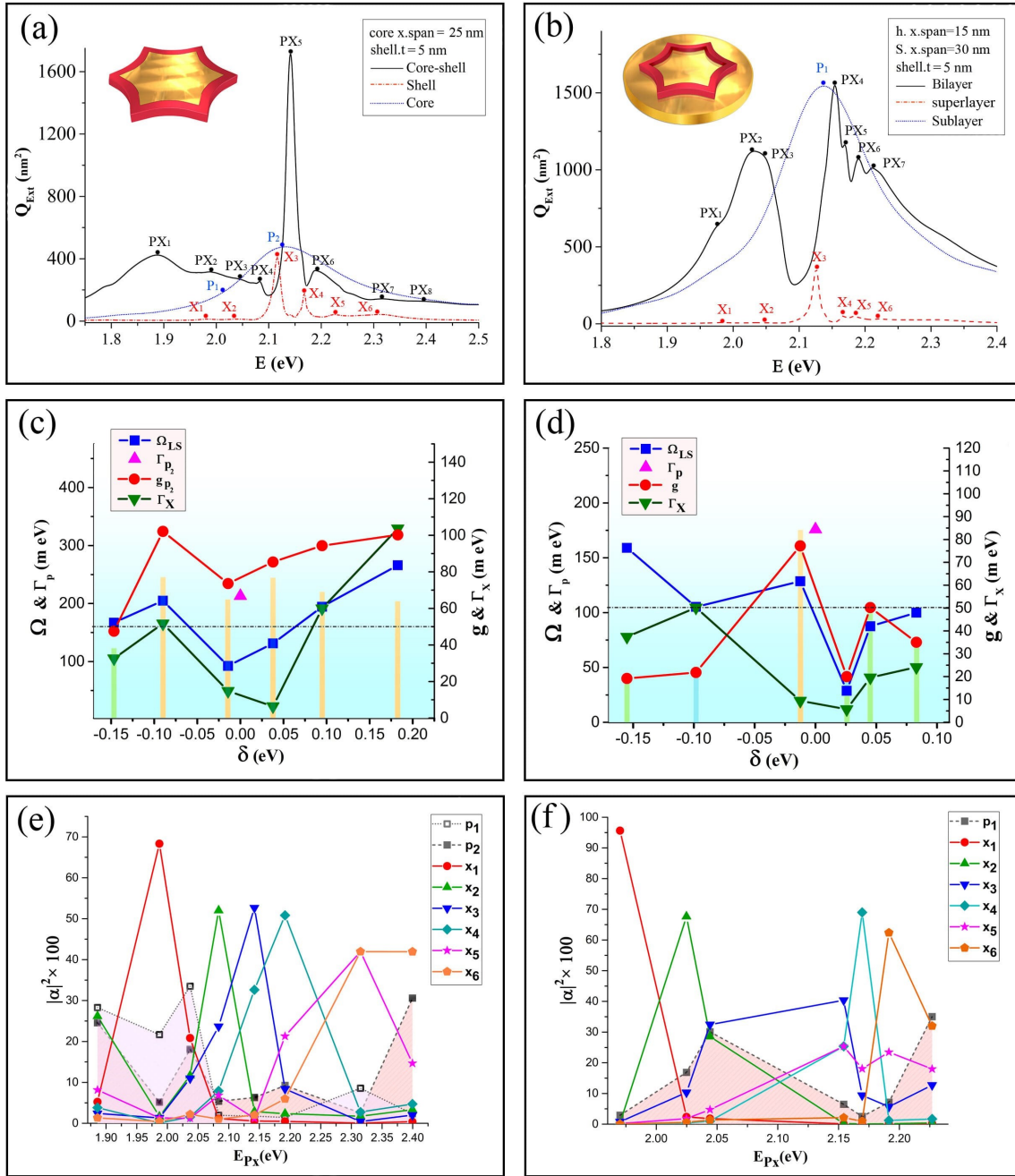


Fig.S13. Same as Fig. S10, except that the extinction spectra was calculated for hexapod supershape nanoparticle.

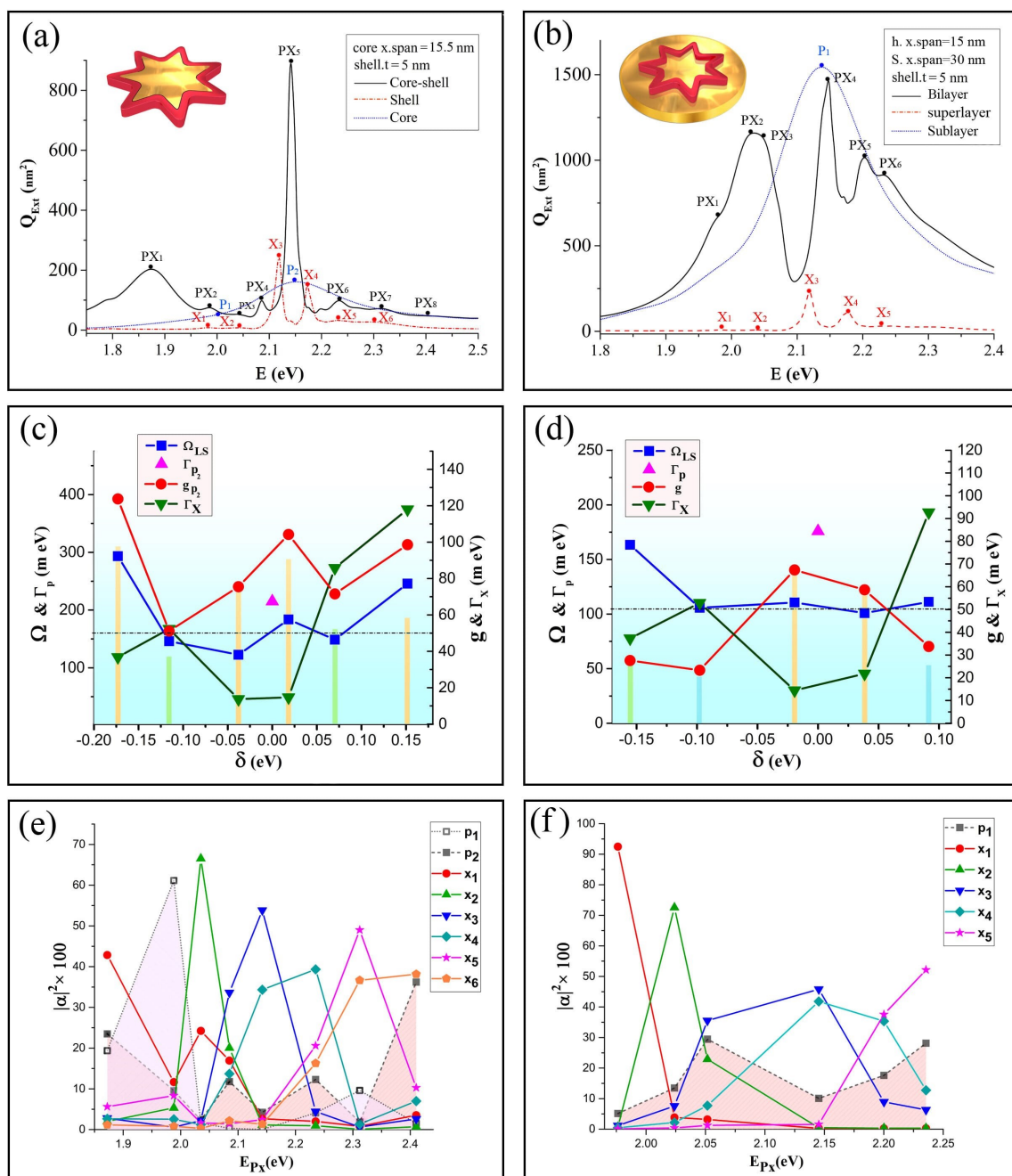


Fig.S14. Same as Fig. S10, except that the extinction spectra was calculated for heptapod supershape nanoparticle.

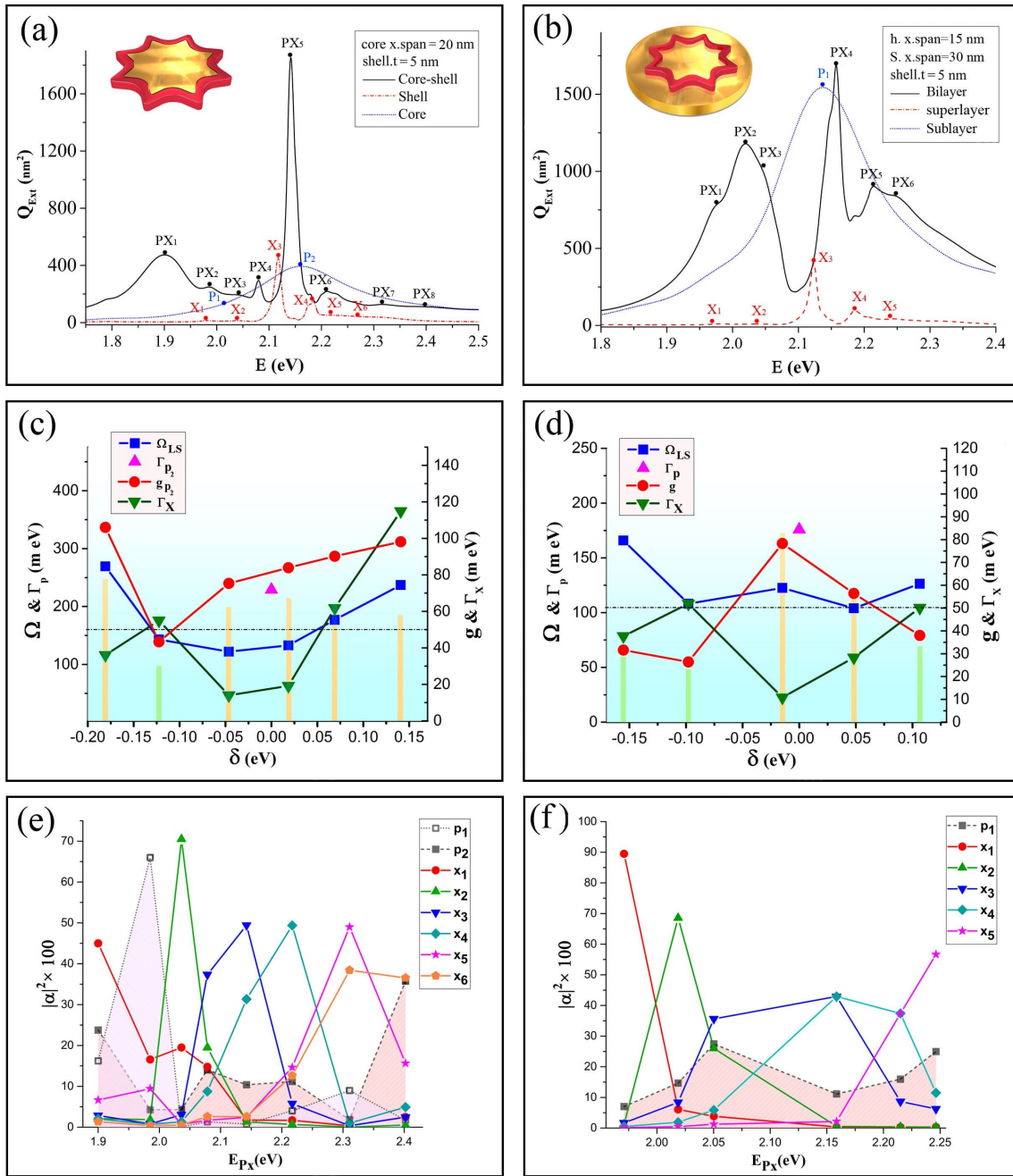


Fig.S15. Same as Fig. S10, except that the extinction spectra was calculated for octapod supershape nanoparticle.

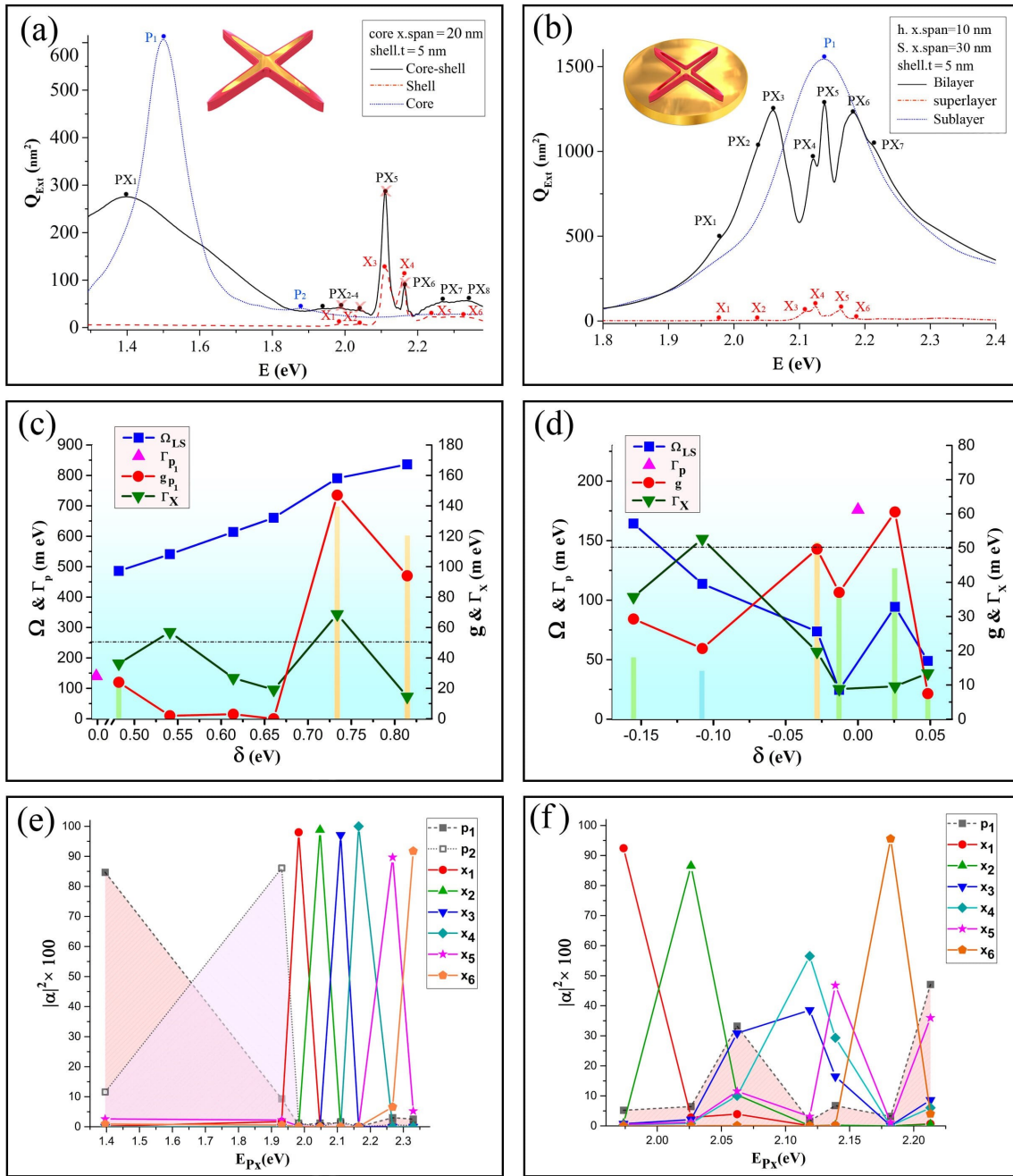


Fig.S16. Same as Fig. S10, except that the extinction spectra was depicted for 4-arms starfish supershape nanoparticle.

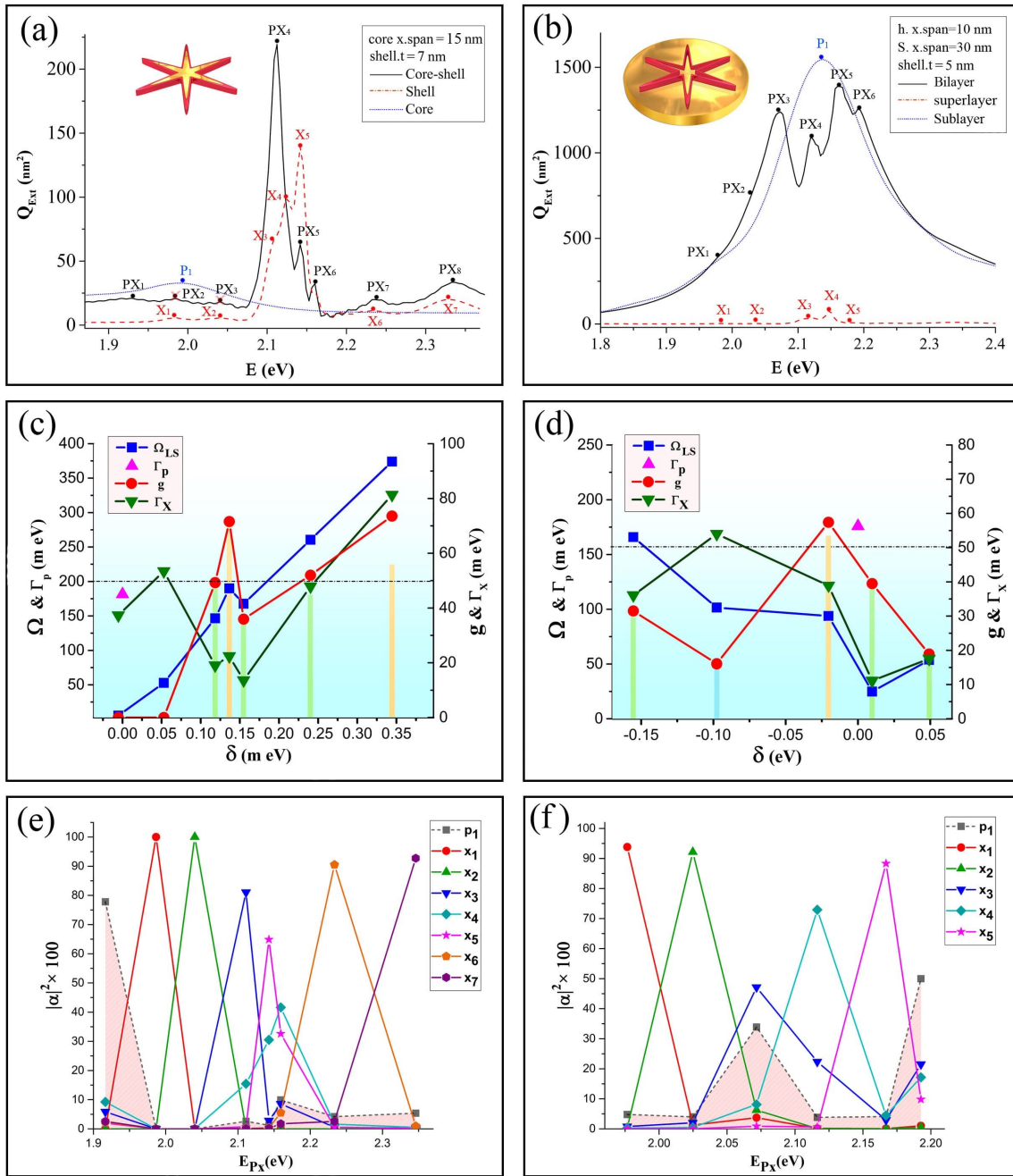


Fig.S17. Same as Fig. S10, except that the extinction spectra was depicted for 6-arms starfish supershape nanoparticle.

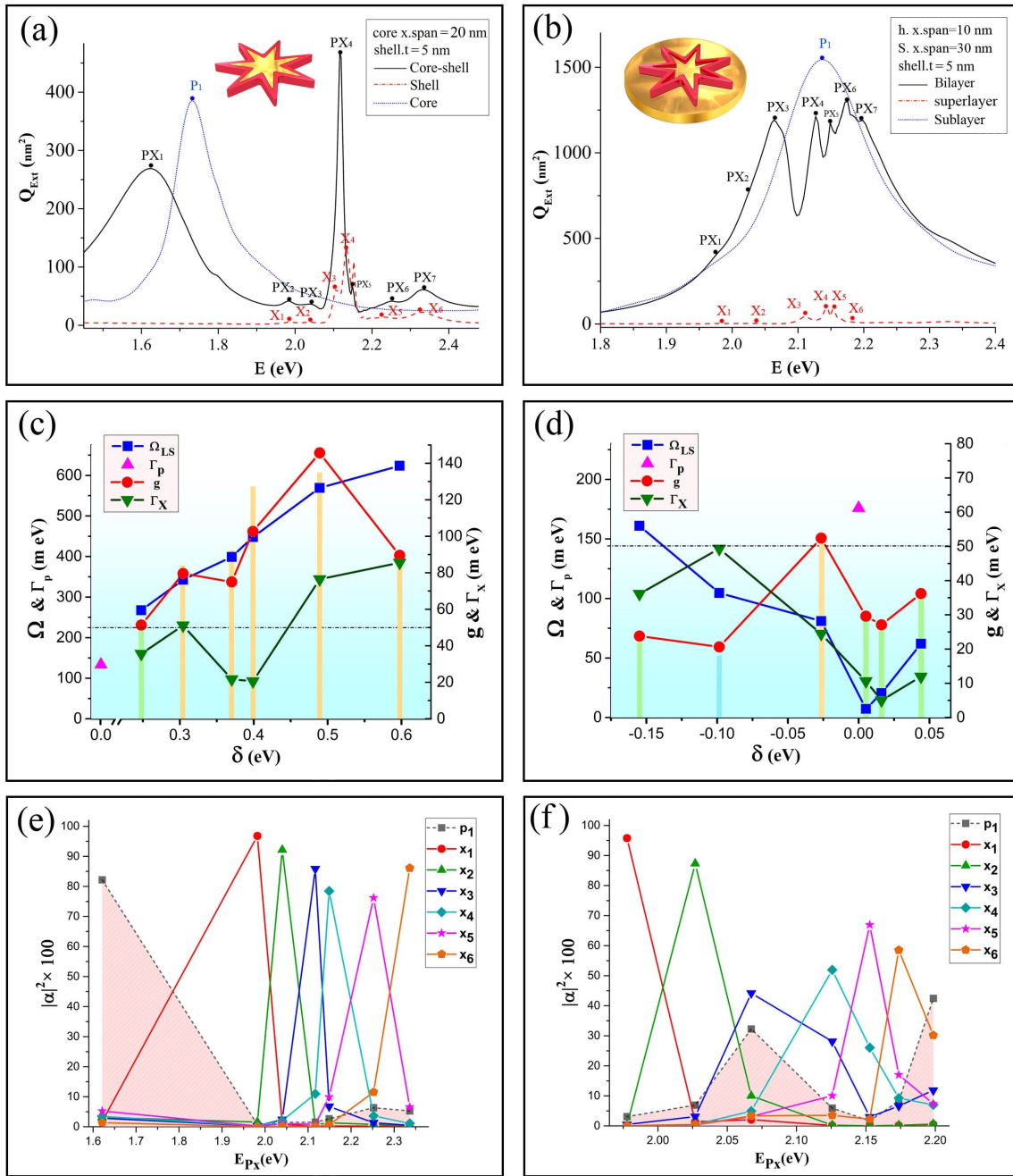


Fig.S18. Same as Fig. S10, except that the extinction spectra was depicted for 7-arms starfish supershape nanoparticle.

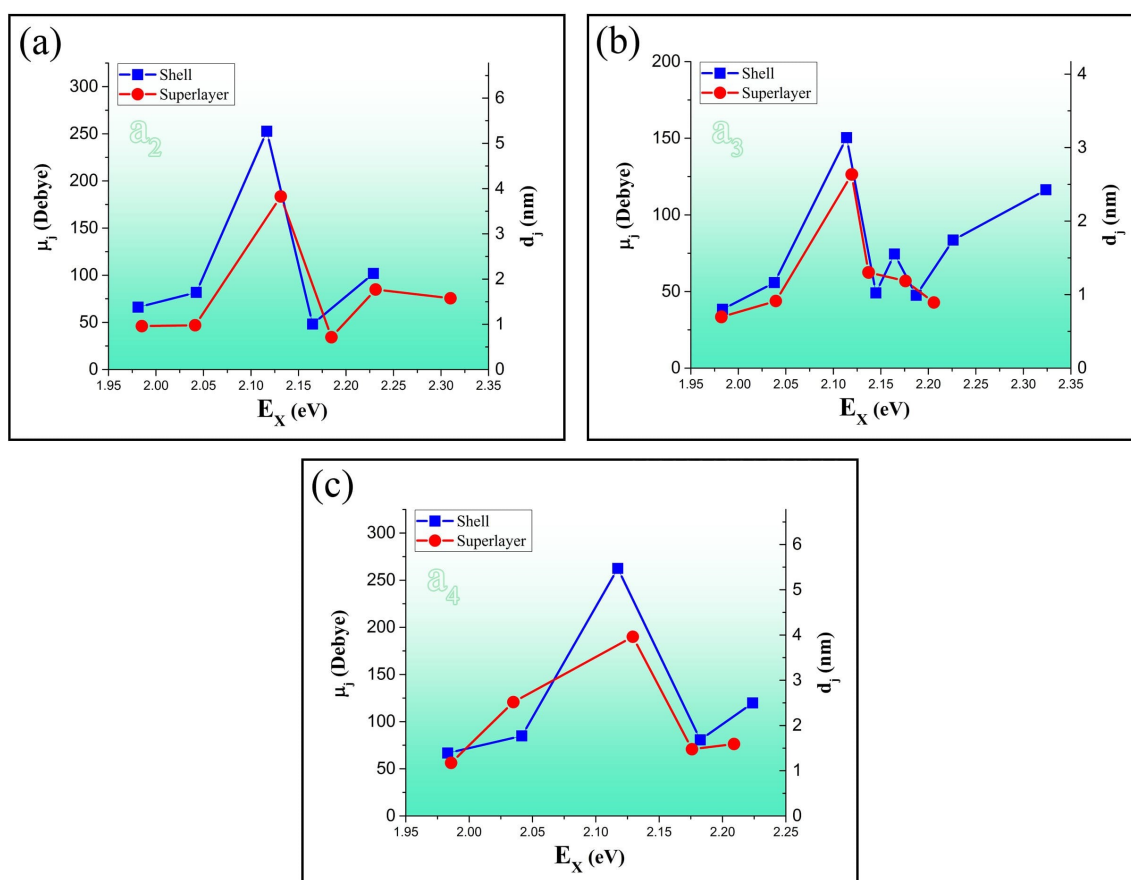


Fig.S19. Transition dipole moment (μ_j) and charge displacement (d_j) of excitons of shell and superlayer in CS and BL nanoparticles, (a) elliptical, (b) triangular, and (c) cuboidal.

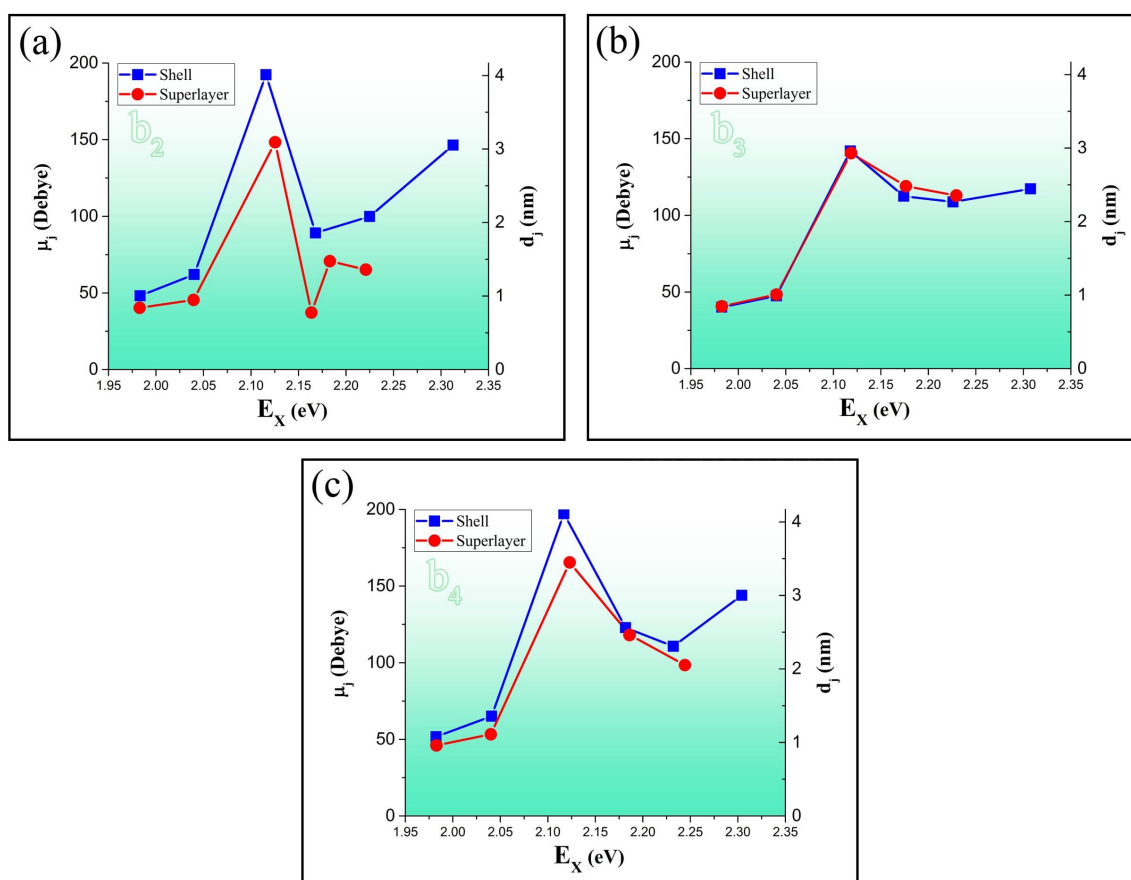


Fig.S20. Transition dipole moment (μ_j) and charge displacement (d_j) of excitons of shell and superlayer in CS and BL nanoparticles, (a) hexapod, (b) heptapod, and (c) octapod.

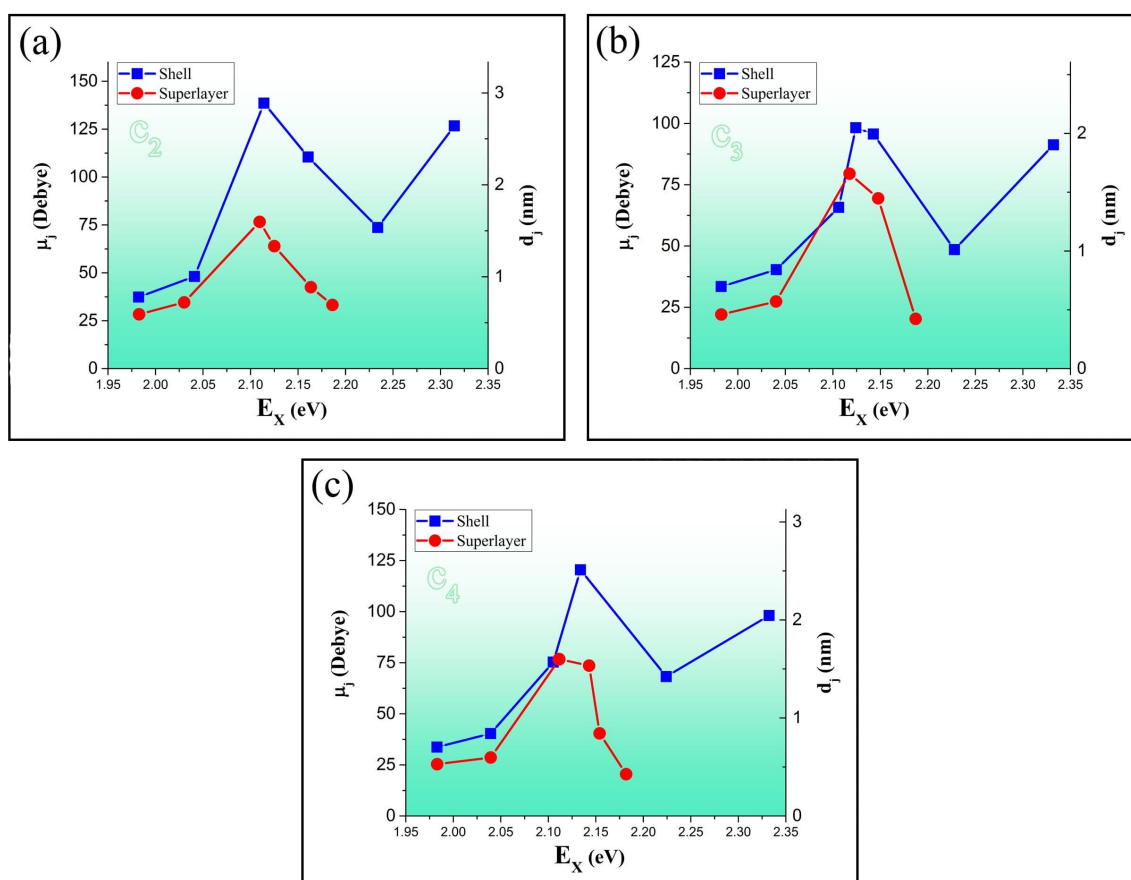


Fig.S21. Transition dipole moment (μ_j) and charge displacement (d_j) of excitons of shell and superlayer in CS and BL nanoparticles, (a)4-arms, (b)6-arms, and (c)7-arms.